Weak decays of medium and heavy Λ hypernuclei

W. M. Alberico, A. De Pace, and G. Garbarino

Dipartimento di Fisica Teorica, Universitá di Torino and INFN, Sezione di Torino, I-10125 Torino, Italy

A. Ramos

Departament d'Estructura i Constituents de la Matèria, Universitat de Barcelona, E-08028 Barcelona, Spain

We have made a new evaluation of the Λ decay width in nuclear matter within the propagator method. Through the local density approximation it is possible to obtain results in finite nuclei. We have also studied the dependence of the widths on the NN and ΛN strong short-range correlations. Using reasonable values for the parameters that control these correlations, as well as realistic nuclear densities and Λ wave functions, we show that it is possible to reproduce the experimental decay rates in a wide range of mass numbers (from medium to heavy hypernuclei); however, the question related to the Γ_n/Γ_p ratio remains open.

I. INTRODUCTION

A hypernucleus is a bound system made of neutrons, protons, and one or more hyperons. Among these *strange nuclei*, those which contain one Λ hyperon are the most stable with respect to the strong interaction and they are the subject of this paper. The study of hypernuclear physics may help in understanding some present problems related, for instance, to some aspects of weak interactions in nuclei or to the origin of the spin-orbit interaction in nuclei. Besides, it is a good instrument to study the role of quark degrees of freedom in the hadron-hadron interactions at short distances and the renormalization properties of pions in the nuclear medium.

Nowadays we know some important features of the YN interaction [1]. For example, at intermediate distances the strong ΛN interaction is weaker than the NN one, and its spin-orbit term is very small. Moreover, the former has a smaller range than the NN one. From the study of mesonic decays of light hypernuclei we have evidence for strongly repulsive cores in the ΛN interaction at short distances [2], which automatically appears in quark-based models [3,4]. These characteristics of the ΛN interaction are important, as we will see, for the evaluation of the decay rates of Λ hypernuclei.

The most interesting hypernuclear decays are those involving weak processes, which directly concern the hyperon. The weak decay of hypernuclei occurs via two channels: the so-called mesonic channel ($\Lambda \to \pi N$) and the nonmesonic one, in which the pion emitted from the weak hadronic vertex is absorbed by one or more nucleons in the medium ($\Lambda N \to NN$, $\Lambda NN \to NNN$, etc.). Obviously, the nonmesonic processes can also be mediated by the exchange of more massive mesons than the pion. The nonmesonic decay is only possible in nuclei and, nowadays, the study of the hypernuclear decay is the only practical way to get information on the weak process $\Lambda N \to NN$, especially on its parity conserving part. In fact, there are no experimental observations for this interaction using lambda beams. However, the inverse reaction $pn \to \Lambda p$ at COSY [5] and RCNP is under study [6].

The free Λ decay is compatible with the $\Delta I = 1/2$ isospin rule, which is also valid for the decay of other hyperons and for kaons (namely, in nonleptonic strangeness changing processes). This rule is based on the experimental observation that the $\Lambda \to \pi^- p$ decay rate is twice the $\Lambda \to \pi^0 n$ one, but it is not yet understood on theoretical grounds. From theoretical calculations like the one in Ref. [7] and from experimental measurements [8] there is some evidence that the $\Delta I = 1/2$ rule is broken in nuclear mesonic decay. However, this is essentially due to shell effects and might not be directly related to the weak process. A recent estimate of $\Delta I = 3/2$ contributions to the $\Lambda N \to NN$ reaction [9] found moderate effects on the hypernuclear decay rates. In the present calculation of the decay rates in nuclei we will assume this rule as valid. The momentum of the final nucleon in $\Lambda \to \pi N$ is about 100 MeV for Λ at rest, so this process is suppressed by the Pauli principle in nuclei (particularly in heavy systems). It is strictly forbidden in infinite nuclear matter (where $k_F^0 \simeq 270$ MeV), but in finite nuclei it can occur because of three important effects: (1) in nuclei the hyperon has a momentum distribution that allows larger momenta for the final nucleon, (2) the final pion feels an attraction by the medium such that for fixed momentum it has a smaller energy than the free one and consequently, due to energy conservation, the final nucleon again has more of a chance to come out above the Fermi surface, and (3) on the nuclear surface the local Fermi momentum is smaller than k_F^0 and favors the decay. Nevertheless, the mesonic width rapidly decreases as the mass number A of the hypernucleus increases [7]. From the study of the mesonic channel it could be possible to extract important information on the pion-nucleus optical potential, which we do not know today in a complete form. In fact, the mesonic rate is very sensitive to the pion self-energy in the medium [7].

The final nucleons in the nonmesonic process $\Lambda N \to NN$ emerge with large momenta ($\simeq 420$ MeV), so this decay is not forbidden by the Pauli principle. On the contrary, apart from very light hypernuclei (the *s*-shell ones), it dominates over the mesonic decay. The nonmesonic channel is characterized by large momentum transfers, so that the details of

the nuclear structure do not have a substantial influence while the NN and ΛN short-range correlations (SRCs) turn out to be very important. There is an anticorrelation between mesonic and nonmesonic decay modes such that the total lifetime is quite stable from light to heavy hypernuclei [8,10]: $\tau_{expt}=(0.5-1)\,\tau_{free}$.

Nowadays, the main problem concerning the weak decay rates is to reproduce the experimental values for the ratio Γ_n/Γ_p between the neutron and the proton induced widths $\Lambda n \to nn$ and $\Lambda p \to np$. The theoretical calculations underestimate the experimental data for all the considered hypernuclei [8,9,11–14]:

$$\left\{\frac{\Gamma_n}{\Gamma_p}\right\}^{th} \ll \left\{\frac{\Gamma_n}{\Gamma_p}\right\}^{expt}, \quad 0.5 \lesssim \left\{\frac{\Gamma_n}{\Gamma_p}\right\}^{expt} \lesssim 2. \quad (1.1)$$

In the one-pion exchange (OPE) approximation the values for this ratio are $0.1-0.2$. On the other hand the OPE model has been able to reproduce the one-body stimulated nonmesonic rates $\Gamma_1=\Gamma_n+\Gamma_p$ for light and medium hypernuclei [11,12,14]. In order to solve this problem many attempts have been made up to now, but without success. Among these we recall the inclusion in the $\Lambda N \to NN$ transition potential of mesons heavier than the pion [11,13,14], the inclusion of interaction terms that violate the $\Delta I=1/2$ rule [9], and the description of the short-range baryon-baryon interaction in terms of quark degrees of freedom [12]. This last calculation is the only one that has found a consistent (but not sufficient) increase of the neutron to proton ratio with respect to the OPE one. However, this calculation is only made for s-shell hypernuclei and their effective quark Lagrangian does not reproduce the experimental ratio between the $\Delta I=1/2$ and $\Delta I=3/2$ transition amplitudes for the Λ free decay.

The analysis of the ratio Γ_n/Γ_p is influenced by the two-nucleon-induced process $\Lambda NN \to NNN$. By assuming that the meson produced in the weak vertex is mainly absorbed by a neutron-proton strongly correlated pair, the three-body process turns out to be $\Lambda np \to nnp$, so that a considerable fraction of the measured neutrons could come from this channel and not only from the $\Lambda n \to nn$ and $\Lambda p \to np$ ones. In this way it might be possible to explain the large experimental Γ_n/Γ_p ratios, which originally have been analyzed without taking into account the two-body-stimulated process. Nevertheless, the situation is far from being clear and simple. The new nonmesonic mode was introduced in Ref. [15] and its calculation was improved in Ref. [16], where the authors found that the inclusion of the new channel would lead to larger values of the Γ_n/Γ_p ratios extracted from the experiment, somehow more in disagreement with theoretical estimates. However, in the hypothesis that only two nucleons from the three-body decay are detected, the reanalysis of the experimental data would lead to smaller ratios [8]. These observations show that Γ_n/Γ_p is sensitive to the energy spectra of the emitted nucleons, whose calculation also requires a careful treatment of the nucleon final state interaction. In Ref. [17] the energy distributions were calculated using a Monte Carlo simulation to describe the final state interactions. A direct comparison of those spectra with the

experimental ones favors Γ_n/Γ_p values around $2-3$ (or higher), in disagreement with the OPE predictions. However, the convenience of measuring the number of protons per decay event was also pointed out. This observable, which can be measured from delayed fission events in the decay of heavy hypernuclei, gives a more reliable ratio Γ_n/Γ_p and is less sensitive to details of the Monte Carlo simulation determining the final shape of the spectra.

In this paper we present a new evaluation of the decay rates for medium to heavy hypernuclei based on the propagator method of Ref. [18], which allows a unified treatment of all the decay channels. The parameters of the model are adjusted to reproduce the nonmesonic width of $^{12}_{\Lambda}C$ and the decay rates of heavier hypernuclei are predicted. We also discuss how the new model affects the energy spectrum of the emitted nucleons, in the hope of obtaining a ratio Γ_n/Γ_p more in agreement with the experimental observation.

The paper is organized as follows. In Sec. II we present the model used for the calculation of the decay rates. Our results are presented and discussed in Sec. III. We first study the sensitivity of the decay rates to the parameters defining the NN and ΛN strong short-range correlations as well as to the nuclear density and Λ wave functions. We then obtain the widths for various hypernuclei and discuss the energy distribution of the nucleons from the weak decays. Our conclusions are given in Sec. IV.
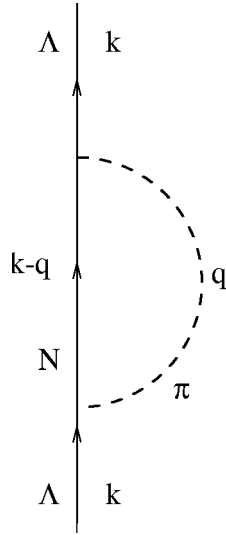
II. PROPAGATOR METHOD

The Λ decay in nuclear systems can be studied in the random phase approximation (RPA) using the propagator method [16,18]. This technique provides a unified picture of the different decay channels and it is equivalent to the standard wave function method (WFM) [19], used by other authors in Refs. [7,9,11,13,14]. The calculation of the widths is usually performed in nuclear matter, and then extended to finite nuclei via the local density approximation (LDA). For the calculation of the mesonic rates the WFM is more reliable than the propagator method in the LDA since this channel is rather sensitive to the shell structure of the hypernucleus, given the small energies involved. Moreover, it is advisable to avoid the use of the LDA for very light systems and we will make the calculation starting from $^{12}_{\Lambda}C$. On the other hand, the propagator method in LDA offers the possibility of calculations over a broad range of mass numbers.

The method was introduced in Ref. [18] and we briefly summarize it here for clarity. The $\Lambda \to \pi N$ effective Lagrangian is

$$\mathcal{L}_{\Lambda \pi N}=Gm_{\pi}^2\bar{\psi}_N(A+B\gamma_5)\boldsymbol{\tau}\cdot\boldsymbol{\phi}_{\pi}\psi_{\Lambda}+\text{H.c.}, \quad (2.1)$$

where the values of the weak coupling constants $G\simeq 2.211\times 10^{-7}/m_{\pi}^2$, $A=1.06$ and $B=-7.10$ are fixed on the free Λ decay. The constants A and B determine the strengths of the parity violating and parity conserving $\Lambda \to \pi N$ amplitudes, respectively. In order to enforce the $\Delta I=1/2$ rule, in Eq. (2.1) the hyperon is assumed to be an isospin spurion with $I_z=-1/2$. To calculate the Λ width in nuclear matter we start with the imaginary part of the Λ self-energy:

FIG. 1. Λ self-energy in nuclear matter.

$$\Gamma_\Lambda = -2\,\mathrm{Im}\,\Sigma_\Lambda\,. \tag{2.2}$$

By the use of Feynman rules, from Fig. 1 it is easy to obtain the Λ self-energy in the following form:

$$\Sigma_\Lambda(k) = 3i(Gm_\pi^2)^2 \int \frac{d^4q}{(2\pi)^4} \left\{ S^2 + \frac{P^2}{m_\pi^2} q^2 \right\}$$

$$\times F_\pi^2(q) G_N(k-q) G_\pi(q). \tag{2.3}$$

Here, $S = A$ and $P = m_\pi B / 2m_N$, while the nucleon and pion propagators in nuclear matter are, respectively,

$$G_N(p) = \frac{\theta(|\boldsymbol{p}| - k_F)}{p_0 - E_N(\boldsymbol{p}) - V_N + i\epsilon} + \frac{\theta(k_F - |\boldsymbol{p}|)}{p_0 - E_N(\boldsymbol{p}) - V_N - i\epsilon} \tag{2.4}$$

and

$$G_\pi(q) = \frac{1}{q_0^2 - \boldsymbol{q}^2 - m_\pi^2 - \Sigma_\pi^*(q)}. \tag{2.5}$$

In the above, $p = (p_0, \boldsymbol{p})$ and $q = (q_0, \boldsymbol{q})$ denote four-vectors, k_F is the Fermi momentum, E_N is the nucleon total free energy, V_N is the nucleon binding energy, and Σ_π^* is the pion proper self-energy in nuclear matter. Moreover, in Eq. (2.3) we have included a monopole form factor for the $\pi\Lambda N$ vertex:

$$F_\pi(q) = \frac{\Lambda_\pi^2 - m_\pi^2}{\Lambda_\pi^2 - q_0^2 + \boldsymbol{q}^2} \tag{2.6}$$

(the same is used for the πNN strong vertex), with cutoff $\Lambda_\pi = 1.2$ GeV. In Fig. 2 we show the lowest order Feynman graphs for the Λ self-energy in nuclear matter. Diagram (a) represents the bare self-energy term, including the effects of Pauli principle and of binding on the intermediate nucleon.
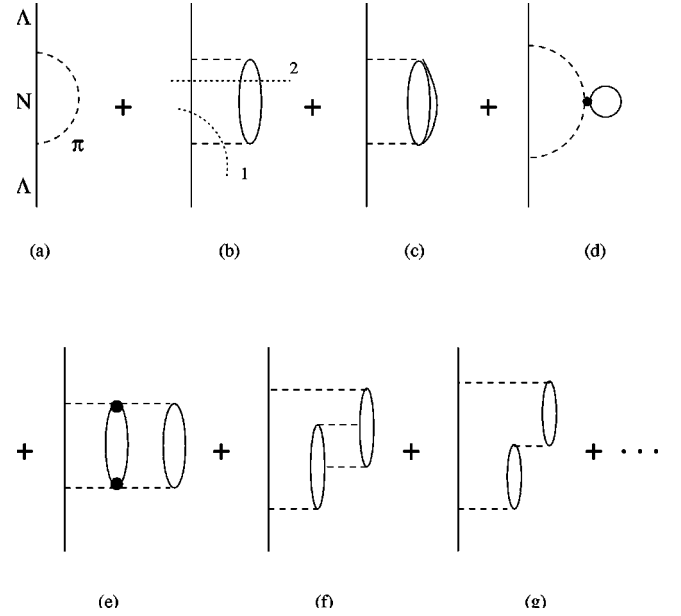

FIG. 2. Lowest order terms for the Λ self-energy in nuclear matter. The meaning of the various diagrams is explained in the text.

In (b) and (c) the pion couples to a particle-hole (p-h) and a Δ-h pairs, respectively. Diagram (d) is an insertion of s-wave pion self-energy at lowest order. In diagram (e) we show a 2p-2h excitation coupled to the pion through s-wave πN interactions. Other 2p-2h excitations, coupled in p wave, are shown in (f), while (g) is a RPA iteration of diagram (b). It is possible to evaluate the integral over q_0 in Eq. (2.3), and the Λ self-energy [Eq. (2.2)] in nuclear matter becomes [18]

$$\Gamma_\Lambda(\boldsymbol{k}, \rho) = -6(Gm_\pi^2)^2 \int \frac{d\boldsymbol{q}}{(2\pi)^3} \theta(|\boldsymbol{k} - \boldsymbol{q}| - k_F)\, \theta(k_0 - E_N$$

$$\times (\boldsymbol{k} - \boldsymbol{q}) - V_N)\mathrm{Im}\,\alpha(q)\big|_{q_0 = k_0 - E_N(\boldsymbol{k} - \boldsymbol{q}) - V_N},$$

$$\tag{2.7}$$

where

$$\alpha(q) = \left\{ S^2 + \frac{P^2}{m_\pi^2} \boldsymbol{q}^2 \right\} F_\pi^2(q) G_\pi^0(q) + \frac{\widetilde{S}^2(q) U(q)}{1 - V_L(q) U(q)}$$

$$+ \frac{\widetilde{P}_L^2(q) U(q)}{1 - V_L(q) U(q)} + 2 \frac{\widetilde{P}_T^2(q) U(q)}{1 - V_T(q) U(q)}. \tag{2.8}$$

In Eq. (2.7) the first θ function forbids intermediate nucleon momenta (see Fig. 1) smaller than the Fermi momentum and the second one requires the pion energy q_0 to be positive. Moreover, the Λ energy, $k_0 = E_\Lambda(k) + V_\Lambda$, contains a binding term. In Eq. (2.8),

$$G_\pi^0(q) = \frac{1}{q_0^2 - \boldsymbol{q}^2 - m_\pi^2} \tag{2.9}$$

is the free pion propagator, while $U(q)$ contains the Lindhard functions for p-h and Δ-h excitations [20] and also accounts for 2p-2h excitations:

$$U(q) = U_{ph}(q) + U_{\Delta h}(q) + U_{2p2h}(q). \qquad (2.10)$$

It appears in Eq. (2.8) within the standard RPA expression. Equation (2.7) depends explicitly and through $U(q)$ on the nuclear matter density $\rho = 2k_F^3/3\pi^2$. The Lindhard functions U_{ph}, $U_{\Delta h}$ are normalized as in Ref. [21] and U_{2p2h} is evaluated as in [16], that is, by calculating the available phase space for 2p-2h excitations and by taking into account the experimental data on pionic atoms. $U(q)$ is related to the pion proper self-energy through

$$\Sigma_\pi^*(q) = \Sigma_\pi^{(p)*}(q) + \Sigma_\pi^{(s)*}(q),$$

$$(2.11)$$

$$\Sigma_\pi^{(p)*}(q) = \frac{\dfrac{f_\pi^2}{m_\pi^2} \boldsymbol{q}^2 F_\pi^2(q) U(q)}{1 - \dfrac{f_\pi^2}{m_\pi^2} g_L(q) U(q)},$$

where the Landau function $g_L(q)$ is given in the Appendix [see Eq. (A12)], and $\Sigma_\pi^{(s)*}$ is the s-wave part of the self-energy. We will use the parametrization of Ref. [22]: $\Sigma_\pi^{(s)*}(q) = -4\pi(1 + m_\pi/m_N)b_0\rho$, with $b_0 = -0.0285/m_\pi$. The function $\Sigma_\pi^{(s)*}$ is real (constant and positive); therefore it contributes only to the mesonic decay [diagram (d) in Fig. 2 is the relative lowest order]. On the contrary, the p-wave self-energy $\Sigma_\pi^{(p)*}$ is complex and attractive [that is, Re $\Sigma_\pi^{(p)*}(q) < 0$].

The pion lines of Fig. 2 have been replaced in Eq. (2.8) by the interactions $\widetilde{S}$, $\widetilde{P}_L$, $\widetilde{P}_T$, V_L, and V_T, whose expressions are given in the Appendix. The functions V_L and V_T represent the (strong) p-h interaction, including π and ρ exchange modulated by the effect of short-range correlations, described by the Landau parameter g', while $\widetilde{S}$, $\widetilde{P}_L$, and $\widetilde{P}_T$ correspond to the lines connecting weak and strong hadronic vertices: they contain the pion and another Landau parameter g'_Λ, which is related to the strong ΛN short-range correlations. Note that in this model ρ exchange enters only in the p-h interaction, but not in the weak vertex. Indeed, it was explicitly shown in Ref. [23] that adding the ρ meson to the pion leads to a reduction of the rate of about $10-15\%$. It was also shown there that the neutron to proton induced ratio Γ_n/Γ_p barely changed from the pion-exchange value. Actually, in a later work [11], which used more realistic NN final state wave functions, it was found that the effect of including the ρ meson in the weak vertex was $\simeq 3\%$. Even the full model employed in that paper, which considered the exchange of all pseudoscalar (π, K, η) and vector mesons (ρ, K^*, ω), yielded a rate that was $\simeq 15\%$ smaller or larger than the OPE value, depending on the coupling constants used in the strong vertices. It is important to stress that the weak couplings, except the ones for the pion, are not known experimentally; in those works they were estimated from soft-meson theorems and SU(6)$_w$ symmetry.

In view of the moderate effect of additional mesons in the weak Lagrangian and of the many poorly known parameters they would bring into the calculation, in this paper we prefer to focus on a simpler but controlled model, such as the OPE one, and defer for a future work the study of the influence of the ρ and other mesons.

The decay widths in finite nuclei are obtained in the LDA. In this approximation, the Fermi momentum is made r dependent (that is, a local Fermi sea of nucleons is introduced) and related again to the nuclear density by

$$k_F(\boldsymbol{r}) = \left\{ \frac{3}{2}\pi^2\rho(\boldsymbol{r}) \right\}^{1/3}. \qquad (2.12)$$

Besides, the nucleon binding potential V_N also becomes r dependent in the LDA. In the Thomas-Fermi approximation we assume

$$\epsilon_F(\boldsymbol{r}) + V_N(\boldsymbol{r}) \equiv \frac{k_F^2(\boldsymbol{r})}{2m_N} + V_N(\boldsymbol{r}) = 0. \qquad (2.13)$$

For the Λ binding energy we use instead the experimental value [24,25].

With these prescriptions we can then evaluate the decay width in finite nuclei by using the semiclassical approximation, through the relation [26,18]

$$\Gamma_\Lambda(\boldsymbol{k}) = \int d\boldsymbol{r} |\psi_\Lambda(\boldsymbol{r})|^2 \Gamma_\Lambda[\boldsymbol{k}, \rho(\boldsymbol{r})], \qquad (2.14)$$

where ψ_Λ is the Λ wave function and $\Gamma_\Lambda[\boldsymbol{k}, \rho(\boldsymbol{r})]$ is given by Eqs. (2.7) and (2.8). $\Gamma_\Lambda(\boldsymbol{k})$, which is not an observable, can be regarded as the $\boldsymbol{k}$ component of the Λ decay width in the nucleus with density $\rho(\boldsymbol{r})$. One can use this relation to estimate the decay rate by introducing an average momentum for the hyperon. More accurately, a further average over the Λ momentum distribution gives the following width:

$$\Gamma_\Lambda = \int d\boldsymbol{k} |\widetilde{\psi}_\Lambda(\boldsymbol{k})|^2 \Gamma_\Lambda(\boldsymbol{k}), \qquad (2.15)$$

which we shall compare with experimental results. On this point we must say that the nonmesonic decay rate is rather independent of the average momentum used in Eq. (2.15) (the variation of this momentum affects the nonmesonic rate by at most 2%). In fact, the nucleons emerging from the nonmesonic processes are very energetic and easily overcome the Pauli blocking. However, the mesonic channel is very much affected by variations of $\boldsymbol{k}$ because the emerging nucleon can more easily overcome the (local) Fermi momentum if the decaying Λ has a larger momentum. For instance, in $^{12}_\Lambda$C, setting the Λ momentum to $\boldsymbol{k} = 0$ we obtain a mesonic rate which is practically zero, while we know from experiment that Γ_M is not negligible in this hypernucleus. Therefore, the further average over $\boldsymbol{k}$ of Eq. (2.15) is more consistent with the physics of the decay.

The propagator method provides a unified picture of the decay widths. The imaginary part of a self-energy diagram requires placing simultaneously on shell the particles of the considered intermediate state. For instance, diagram (b) in

Fig. 2 has two sources of imaginary part. One comes from cut 1, where the nucleon and the pion are placed on shell. This term contributes to the mesonic channel: the final pion interacts with the medium through a p-h excitation and then escapes from the nucleus. Diagram (b) and further iterations lead to a renormalization of the pion in the medium which increases the mesonic rate by about two orders of magnitude in heavy nuclei [18]. Cut 2 in Fig. 2(b) places a nucleon and a p-h pair on shell, so it is the lowest order contribution to the physical process $\Lambda N \to NN$.

The mesonic width Γ_M is calculated from

$$\alpha(q) = \left\{ S^2 + \frac{P^2}{m_\pi^2} q^2 \right\} F_\pi^2(q) G_\pi(q), \qquad (2.16)$$

by omitting $\text{Im} \Sigma_\pi^*$ in G_π, namely, by replacing

$$\text{Im} \, G_\pi(q) \to -\pi \delta(q_0^2 - q^2 - m_\pi^2 - \text{Re} \, \Sigma_\pi^*(q)). \quad (2.17)$$

The one-body-induced nonmesonic decay rate Γ_1 is obtained by substituting in Eqs. (2.7) and (2.8)

$$\text{Im} \frac{U(q)}{1 - V_{L,T}(q) U(q)} \to \frac{\text{Im} \, U_{ph}(q)}{|1 - V_{L,T}(q) U(q)|^2}, \quad (2.18)$$

that is, by omitting the imaginary parts of $U_{\Delta h}$ and U_{2p2h} in the numerator. Indeed $\text{Im} \, U_{\Delta h}$ accounts for the $\Delta \to \pi N$ decay width, thus representing a contribution to the mesonic decay. There is no overlap between $\text{Im} \, U_{ph}(q)$ and the pole $q_0 = \omega(q)$ in Eq. (2.17), so the separation of the mesonic and two-body nonmesonic channels is unambiguous. The renormalized pion pole in Eq. (2.16) is given by the dispersion relation

$$\omega^2(q) - q^2 - m_\pi^2 - \text{Re} \, \Sigma_\pi^*[\omega(q), q] = 0, \qquad (2.19)$$

with the constraint

$$q_0 = k_0 - E_N(k - q) - V_N. \qquad (2.20)$$

At the pion pole $\text{Im} \, U_{2p2h} \neq 0$; thus the two-body-induced nonmesonic width Γ_2 cannot be calculated using the prescription (2.18) with U_{2p2h} instead of U_{ph} in the numerator of the right-hand side (RHS). Part of the decay rate calculated in this way it is due to excitations of the renormalized pion and contributes to Γ_M. The three-body nonmesonic rate is then calculated by subtracting Γ_M and Γ_1 from the total rate Γ_{TOT}, which we get via the full expression for α [Eq. (2.8)].

III. RESULTS AND DISCUSSION

Let us now discuss the numerical results one can obtain from the above illustrated formalism. We shall first study the influence of short-range correlations and the Λ wave function on the decay width of $^{12}_\Lambda C$, which will be used as a testing ground for the theoretical framework in order to fix the parameters of our model. We will then obtain the decay widths of heavier hypernuclei and we will explore whether

the refined model influences the energy distribution of the emitted particles, following the Monte Carlo procedure of Ref. [17].

In order to evaluate the width (2.14) one needs to specify the nuclear density and the wave function for the Λ. The former is assumed to be a Fermi distribution:

$$\rho_A(r) = \frac{\rho_0(A)}{1 + e^{[r - R(A)]/a}}$$

$$\times \left[\rho_0(A) = \frac{A}{\frac{4}{3} \pi R^3(A) \{ 1 + [\pi a / R(A)]^2 \}} \right],$$
$$(3.1)$$

with radius $R(A) = 1.12 A^{1/3} - 0.86 A^{-1/3}$ fm and thickness $a = 0.52$ fm. We recall that the present calculation is performed in symmetric nuclear matter, without distinguishing (in heavy nuclei) between the proton and neutron density distributions. Moreover, the LDA is a good approximation to obtain the general trend of the A dependence, but will not account for any shell-structure effect. Concerning the Λ wave function, it is obtained from a Woods-Saxon (WS) well which exactly reproduces the first two single-particle eigenvalues (s and p levels) measured in Λ hypernuclei.

A. Short-range correlations and Λ wave function

A crucial ingredient in the calculation of the decay widths is the short-range part of the strong NN and ΛN interactions. They are expressed by the functions $g_{L,T}(q)$ and $g_{L,T}^\Lambda(q)$, which are reported in the Appendix and contain the Landau parameters g' and g_Λ'. No experimental information is available on g_Λ', while many constraints have been set on g', for example, by the well-known quenching of the Gamow-Teller resonance. Realistic values of g', within the framework of the ring approximation, are in the range $0.6 - 0.7$ [27]. However, in the present context g' correlates not only p-h pairs but also p-h with 2p-2h states. In order to fix these parameters we shall compare our calculations with the experimental nonmesonic width of $^{12}_\Lambda C$.

In Fig. 3 we see how the total nonmesonic width for carbon depends on the Landau parameters. The rate decreases as g' increases. This characteristic is well established in the RPA. Moreover, fixing g', there is a minimum for $g_\Lambda' \simeq 0.4$ (almost independent of the value of g'). This is due to the fact that for $g_\Lambda' \lesssim 0.4$ the longitudinal p-wave contribution in Eq. (2.8) dominates over the transverse one and the opposite occurs for $g_\Lambda' \gtrsim 0.4$. We also recall that the s-wave interactions are independent of g_Λ' [Eq. (A10)]. Moreover, the longitudinal p-wave $\Lambda N \to NN$ interaction [Eq. (A8)] contains the pion exchange plus SRCs, while the transverse p-wave $\Lambda N \to NN$ interaction [Eq. (A9)] only contains repulsive correlations, so with increasing g_Λ' the p-wave longitudinal contribution to the width decreases, while the p-wave transverse part increases. From Fig. 3 we see that there is a broad range of choices of g' and g_Λ' values which fit the experimental band. The latter represents the nonmesonic decay width which is compatible with both the BNL [28] and KEK [29]
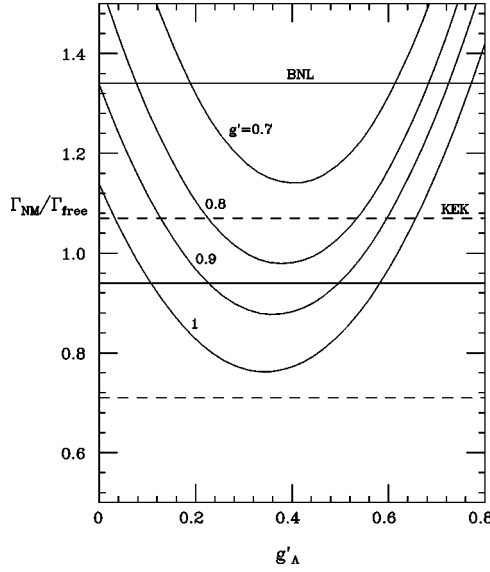
FIG. 3. Dependence of the nonmesonic width on the Landau parameters g' and g'_Λ for $^{12}_\Lambda$C. The experimental value from BNL [28] (KEK [29]) lies in between the horizontal solid (dashed) lines.

experiments. One should notice that the theoretical curves reported in Fig. 3 contain the contribution of the three-body process; should the latter be neglected (ring approximation), then one could get equivalent results with g' values smaller than the ones reported in the figure (typically $\Delta g' \simeq -0.1$). The phenomenology of the (e,e') quasielastic scattering suggests, in the ring approximation, typical values of g' in the range $0.6-0.7$. Here, by taking into account also 2p-2h contributions, we have to adopt ''equivalent'' g' values larger than in ring approximation. From Fig. 3, the experimental band appears to be compatible with g' in the range $0.75-0.85$ and g'_Λ in the range $0.3-0.5$. On the other hand, the new and more accurate KEK results [32,33] set an upper limit of $\simeq 1.03$ for the nonmesonic width, which practically forces us to chose $g' \simeq 0.8$ and g'_Λ in the above-mentioned interval. Considering that the decay rate does not change dramatically in this range, the value $g'_\Lambda = 0.4$ seems to be a good choice.

We note that the values used in Ref. [16], namely, $g' = 0.615$ and $g'_\Lambda = 0.62$, would yield $\Gamma_1 = 1.26$ and $\Gamma_2 = 0.25$, adding to a nonmesonic width $\Gamma_{NM} = 1.51$, which is 50% larger than the experimental one. Thus the analysis performed here shows that the present data for $^{12}_\Lambda$C favor a somewhat different but still reasonable g' value.

We shall now illustrate the sensitivity of our calculation to the Λ wave function in $^{12}_\Lambda$C. In addition to the WS well

that reproduces the s and p levels, we also use a harmonic oscillator wave function with an ''empirical'' frequency ω [24,25], again obtained from the s-p energy shift, the WS wave function of Dover *et al.* [30], and the microscopic wave function calculated from a nonlocal self-energy using a realistic YN interaction in Ref. [31]. The results are shown in Table I, where they are compared with the experimental data from BNL [28] and KEK [29,32,33].

By construction, the chosen g' and g'_Λ reproduce the experimental decay widths using the WS wave function which gives the right s and p levels in $^{12}_\Lambda$C. We note that it is possible to generate the microscopic wave function of Ref. [31] for carbon via a local hyperon-nucleus WS potential with radius 2.92 fm and depth -23 MeV. Although this potential reproduces fairly well the experimental s level for the Λ in $^{12}_\Lambda$C, it does not reproduce the p level. In this work we prefer to use a completely phenomenological Λ-nucleus potential that can easily be extended to heavier nuclei and reproduces the experimental Λ single particle levels as well as possible. Except for s-shell hypernuclei, where experimental data require Λ-nucleus potentials with a repulsive core at short distances [2], the Λ binding energies have been well reproduced by WS potentials. We thus use a WS potential with fixed diffuseness ($a=0.6$ fm) and adjust the radius and depth to reproduce the s and p Λ levels. The parameters of the potential for carbon are $R=2.27$ fm and $V_0=-32$ MeV.

To analyze the results of Table I, we note that the microscopic wave function is substantially more extended than all the other wave functions used in the present study. The Dover parameters [30], namely, $R=2.71$ fm and $V_0=-28$ MeV, give rise to a Λ wave function that is somewhat more extended than the new WS one but is very similar to that obtained from a harmonic oscillator with a frequency of 10.9 MeV, adjusted to the s-p energy shift in carbon. Consequently, the nonmesonic width from the Dover's wave function is very similar to the one obtained from the harmonic oscillator and slightly smaller than the new WS one. The microscopic wave function predicts the smallest nonmesonic widths due to the more extended Λ wave function, which explores regions of lower density and thus has a smaller probability of interacting with one or more nucleons. From Table I we also see that, against intuition, the mesonic width is quite insensitive to the Λ wave function. On this point we recall that the more extended the Λ wave function is in r space, the larger is the mesonic width, since the Pauli blocking effects on the emitted nucleon are reduced. However, the integral over momenta in Eq. (2.15) is weighted by the mo-

TABLE I. Wave function sensitivity.

$^{12}_\Lambda$C	h.o.	Dover	New WS	Microscopic	BNL [28]	KEK [29]	KEK new [32,33]
Γ_M	0.26	0.25	0.25	0.25	0.11 ± 0.27	0.36 ± 0.15	>0.11
Γ_1	0.78	0.77	0.82	0.69			
Γ_2	0.15	0.15	0.16	0.13			
Γ_{NM}	0.93	0.92	0.98	0.81	1.14 ± 0.20	0.89 ± 0.18	<1.03
Γ_{TOT}	1.19	1.17	1.23	1.06	1.25 ± 0.18	1.25 ± 0.18	1.14 ± 0.08

TABLE II. WS parameters.

$^{A+1}_{\Lambda}Z$	R (fm)	V_0 (MeV)
$^{12}_{\Lambda}$C	2.27	-32.0
$^{28}_{\Lambda}$Si	3.33	-29.5
$^{40}_{\Lambda}$Ca	4.07	-28.0
$^{56}_{\Lambda}$Fe	4.21	-29.0
$^{89}_{\Lambda}$Y	5.07	-28.5
$^{139}_{\Lambda}$La	6.81	-27.5
$^{208}_{\Lambda}$Pb	5.65	-32.0

mentum distribution $|\tilde{\psi}_{\Lambda}(k)|^2$, which correspondingly tends to cancel the above-mentioned effect: as a result Γ_M is insensitive to the different wave functions used in the calculation. In summary, different (but realistic) Λ wave functions give rise to total decay widths which may differ at most by 15%.

B. Decay widths of medium-heavy hypernuclei

Using the new WS wave functions and the Landau parameters $g'=0.8$ and $g'_{\Lambda}=0.4$ we have extended the calculation to heavier hypernuclei. We note that, in order to reproduce the experimental s and p levels for the hyperon, we must use potentials with nearly constant depth, around $28-32$ MeV, from medium to heavy hypernuclei (radii and depths of the used WS potentials are quoted in Table II).

Our results are shown in Table III. We observe that the mesonic rate rapidly vanishes by increasing the mass number A. This is well known and it is related to the decreasing phase space allowed for the mesonic channel and to smaller overlaps between the Λ wave function ψ_{Λ} and the nuclear surface, as A increases. The two-body-induced decay is rather independent of the hypernuclear dimension and it is about 15% of the total width. Previous works [15,16] gave more emphasis on this new channel, without, however, reproducing the experimental results. The total width is also nearly constant with A, as we already know from the experiment. In Fig. 4 we compare the results from Table III with recent (after 1990) experimental data for nonmesonic decay [28,29,32,34–36].

Nevertheless, we recall that the data for nuclei from $^{28}_{\Lambda}$Si on refer to the total width. However, as can be seen from Table III, $\Gamma_M(^{28}_{\Lambda}$Si$)/\Gamma_{NM}(^{28}_{\Lambda}Si)\simeq 6\times 10^{-2}$ and this ratio rapidly decreases with A. The theoretical results are in good

TABLE III. Decay rates.

$^{A+1}_{\Lambda}Z$	Γ_M	Γ_1	Γ_2	Γ_{TOT}
$^{12}_{\Lambda}$C	0.25	0.82	0.16	1.23
$^{28}_{\Lambda}$Si	0.07	1.02	0.21	1.30
$^{40}_{\Lambda}$Ca	0.03	1.05	0.21	1.29
$^{56}_{\Lambda}$Fe	0.01	1.12	0.21	1.35
$^{89}_{\Lambda}$Y	6×10^{-3}	1.16	0.22	1.38
$^{139}_{\Lambda}$La	6×10^{-3}	1.14	0.18	1.33
$^{208}_{\Lambda}$Pb	1×10^{-4}	1.21	0.19	1.40

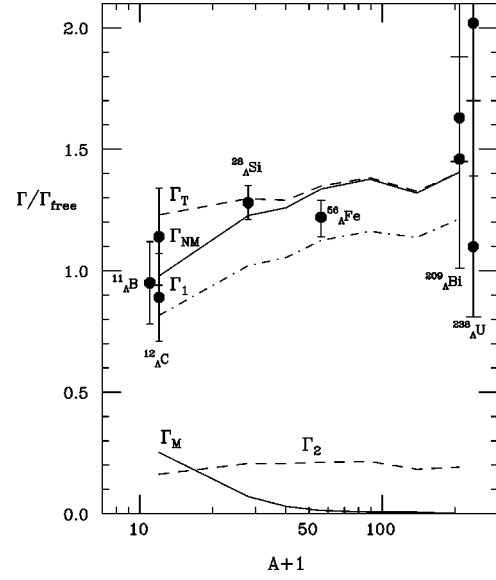FIG. 4. Λ decay widths in finite nuclei as a function of the mass number A.

agreement with the data (which, on the other hand, have large error bars) over the whole hypernuclear mass range explored. Moreover, we also see how the saturation of the $\Lambda N\rightarrow NN$ interaction in nuclei is well reproduced.

One of the open problems in the study of weak hypernuclear decays is to understand the large experimental value of the ratio Γ_n/Γ_p which most of the present theories fail to reproduce. Only the quark model of Ref. [12] predicts an enhanced ratio, although it cannot describe both mesonic and nonmesonic decays from the same basic quark Hamiltonian. However, we have to recall that the data for Γ_n/Γ_p have a large uncertainty and they have been analyzed without taking into account the three-body decay mechanism. The study of Ref. [16] showed that, even if the three-body reaction is only about 15% of the total decay rate, this mechanism influences the analysis of the data determining the ratio Γ_n/Γ_p. The energy spectra of neutrons and protons from the nonmesonic decay mechanisms were calculated in Ref. [17]. The momentum distributions of the primary nucleons were determined from the propagator method and a subsequent Monte Carlo simulation was used to account for the final state interactions. It was shown that the shape of the proton spectrum was sensitive to the ratio Γ_n/Γ_p. In fact, the protons from the three-nucleon mechanism appeared mainly at low energies, while those from the two-body process peaked around 75 MeV. Since the experimental spectra show a fair amount of protons in the low energy region, they would favor a relatively larger three-body decay rate or, conversely, a reduced number of protons from the two-body process. Consequently, the experimental spectra are compatible with values for Γ_n/Γ_p around $2-3$, in strong contradiction with the present theories.

The excellent agreement with the experimental decay rates of medium to heavy hypernuclei obtained here from the propagator method with modified parameters makes it worthwhile to explore the predictions for the nucleon spectra. The question is whether this modified model affects the momen-
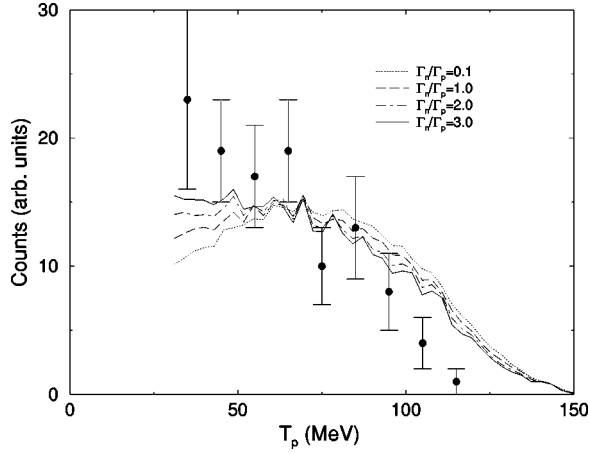
FIG. 5. Proton spectrum from the decay of $^{12}_{\Lambda}$C for various values of Γ_n/Γ_p. The experimental data are taken from Ref. [28].

tum distribution of the primary emitted nucleons strongly enough, such that good agreement with the experimental proton spectra is obtained without the need for very large values for Γ_n/Γ_p. We have thus generated the nucleon spectra from the decay of several hypernuclei using the Monte Carlo simulation of Ref. [17] but with our modified g' and g'_{Λ} parameters and our more realistic nuclear density and Λ wave functions. The spectra obtained for various values of Γ_n/Γ_p, used as a free parameter in the approach of Ref. [17], are compared with the BNL experimental data [28] in Fig. 5.

We observe that, although the nonmesonic widths are smaller by about 35% than those of Refs. [16,17], the resulting nucleon spectra, once they are normalized to the same total width, are practically identical. The reason is that the ratio Γ_2/Γ_1 of two-body-induced versus one-body-induced decay rates is essentially the same in both models (between 0.2 and 0.15 from medium to heavy hypernuclei), and the momentum distributions for the primary emitted protons are also very similar. As a consequence, the conclusions drawn in Ref. [17] still hold and the present calculation would also favor very large values of Γ_n/Γ_p.

Therefore, the origin of the discrepancy between theory and experiment for the ratio Γ_n/Γ_p still needs to be resolved. From the theoretical side, there is still room for improving the numerical simulation of final state interactions. In particular, Coulomb distortions and the evaporating processes need to be incorporated. We think that the evaporating process is an important ingredient which increases the nucleon spectra at low energies. Maybe this contribution is so important that there is no need for high Γ_n/Γ_p values. On the experimental side, although new spectra are now available [29,32], they have not been corrected for energy losses inside the target or detector, so a direct comparison with the theoretical predictions is not yet possible. Attempts to incorporate these corrections by combining a theoretical model for the nucleon rescattering in the nucleus with a simulation of the energy losses in the experimental setup are now being pursued [37]. These efforts call for newer improved theoretical models that incorporate those final state interaction effects missing in Ref. [17]. On the other hand, a forward step

towards a clean extraction of the ratio Γ_n/Γ_p would be obtained if the nucleons from the different nonmesonic processes $\Lambda N \to NN$ and $\Lambda NN \to NNN$ were disentagled. Through the measurement of the coincident spectra of the outgoing nucleons, it could be possible, in the near future, to split the nonmesonic decay width into its two components Γ_1 and Γ_2 [38] and obtain a cleaner measurement of the ratio Γ_n/Γ_p.

IV. CONCLUSIONS

Using the propagator method in the local density approximation, in this paper we made a new evaluation of the Λ decay widths in nuclei. Special attention has been devoted to the study of the NN and ΛN short-range interactions and realistic nuclear densities and Λ wave functions were used. We have adjusted the parameters that control the short-range correlations to reproduce the experimental decay widths of $^{12}_{\Lambda}$C. Then, the calculation has been extended to heavier hypernuclei, up to $^{208}_{\Lambda}$Pb. We reproduce for the first time the experimental nonmesonic decay widths from medium to heavy Λ hypernuclei and saturation of the $\Lambda N \to NN$ interaction is observed.

The energetic spectra of emitted nucleons calculated using the propagator method with modified parameters (describing the energy distributions of primary nucleons) and Monte Carlo simulation (accounting for the final state interactions) do not change appreciably with respect to those calculated in Ref. [17]. The reason is that, in spite of the fact that the nonmesonic decay widths Γ_1 and Γ_2 are sizably reduced (by about 35%) with respect to those of Ref. [17], the ratio Γ_1/Γ_2 is not altered, and the momentum distributions of primary nucleons are very similar to the previous calculation. So the conclusion drawn in Ref. [17] still holds: a comparision of the calculated spectra with the experimental one favors Γ_n/Γ_p ratios around $2-3$ (or higher), in disagreement with the OPE predictions. On the other hand, we have to recall that for a clean experimental extraction of the Γ_n/Γ_p ratio it is very important to identify the nucleons which come out from the different nonmesonic processes [39].

APPENDIX SPIN-ISOSPIN NN AND $\Lambda N \to NN$ INTERACTIONS

In this appendix we show how the repulsive NN and ΛN short-range correlations are implemented in the $NN \to NN$ and $\Lambda N \to NN$ interactions. The process $NN \to NN$ can be described through an effective potential given by

$$G(r) = g(r)V(r). \tag{A1}$$

Here $g(r)$ is a two-body correlation function, which vanishes as $r \to 0$ and goes to 1 as $r \to \infty$, while $V(r)$ is a meson-exchange potential which in our case contains π and ρ exchange: $V = V_\pi + V_\rho$. A practical form for $g(r)$ is [27]

$$g(r) = 1 - j_0(q_c r). \tag{A2}$$

With $q_c \simeq 780$ MeV one gets a good reproduction of realistic NN correlation functions obtained from G-matrix calculations. The inverse of q_c is indicative of the hard-core radius of the interaction. Since there are no experimental indications, we use the same correlation momentum for the ΛN interaction. On the other hand, we recall that q_c is not necessarily the same in the two cases, given the different nature of the repulsive forces. Using the correlation function (A2) it is easy to get the effective interaction, Eq. (A1), in momentum space. It reads

$$G_{NN}(q) = V_\pi(q) + V_\rho(q) + \frac{f_\pi^2}{m_\pi^2}\{g_L(q)\hat{q}_i\hat{q}_j$$

$$+ g_T(q)(\delta_{ij} - \hat{q}_i\hat{q}_j)\}\sigma_i\sigma_j\boldsymbol{\tau}\cdot\boldsymbol{\tau}, \tag{A3}$$

where the SRCs are embodied in the correlation functions g_L and g_T. The spin-isospin $NN \to NN$ interaction can be separated into a spin-longitudinal and a spin-transverse parts, as follows:

$$G_{NN}(q) = \{V_L(q)\hat{q}_i\hat{q}_j + V_T(q)(\delta_{ij} - \hat{q}_i\hat{q}_j)\}\sigma_i\sigma_j\boldsymbol{\tau}\cdot\boldsymbol{\tau}$$

$$\times (\hat{q}_i = q_i/|\boldsymbol{q}|), \tag{A4}$$

where

$$V_L(q) = \frac{f_\pi^2}{m_\pi^2}\{\boldsymbol{q}^2 F_\pi^2(q)G_\pi^0(q) + g_L(q)\}, \tag{A5}$$

$$V_T(q) = \frac{f_\pi^2}{m_\pi^2}\{\boldsymbol{q}^2 C_\rho F_\rho^2(q)G_\rho^0(q) + g_T(q)\}. \tag{A6}$$

In the above F_ρ is the ρNN form factor [Eq. (2.6) with cutoff $\Lambda_\rho = 2.5$ GeV], and $G_\rho^0 = 1/(q_0^2 - \boldsymbol{q}^2 - m_\rho^2)$ is the ρ free propagator.

The $\Lambda N \to NN$ transition potential, modified by the effect of the strong ΛN correlations, splits into a p-wave (again longitudinal and transverse) part

$$G_{\Lambda N \to NN}(q) = \{\tilde{P}_L(q)\hat{q}_i\hat{q}_j + \tilde{P}_T(q)(\delta_{ij} - \hat{q}_i\hat{q}_j)\}\sigma_i\sigma_j\boldsymbol{\tau}\cdot\boldsymbol{\tau}, \tag{A7}$$

with

$$\tilde{P}_L(q) = \frac{f_\pi}{m_\pi}\frac{P}{m_\pi}\{\boldsymbol{q}^2 F_\pi^2(q)G_\pi^0(q) + g_L^\Lambda(q)\}, \tag{A8}$$

$$\tilde{P}_T(q) = \frac{f_\pi}{m_\pi}\frac{P}{m_\pi}g_T^\Lambda(q), \tag{A9}$$

and an s-wave part

$$\tilde{S}(q) = \frac{f_\pi}{m_\pi}S\{F_\pi^2(q)G_\pi^0(q) - \tilde{F}_\pi^2(q)\tilde{G}_\pi^0(q)\}|\boldsymbol{q}|. \tag{A10}$$

Note that in the absence of *strong* ΛN correlations the *weak* potential in p wave is that of Eqs. (A7), (A8), and (A9) setting $g_{L,T}^\Lambda(q) = 0$. The s wave would be given by Eq. (A10) omitting the second term on the RHS. As stated after Eq. (A2), we include the *strong* ΛN correlations using the same correlation function $g(r)$ of Eqs. (A1) and (A2) used in the NN case. Moreover, we point out that the meson-exchange potential $V(\boldsymbol{r})$ of Eq. (A1) is $V = V_\pi + V_\rho$ when we calculate the effective potential G_{NN} while it is $V = V_\pi$ for $G_{\Lambda N \to NN}$. Form factors and propagators with a tilde in Eq. (A10) imply that they are calculated changing $q^2 \to q^2 + q_c^2$. The parameter C_ρ in Eq. (A6) is given by

$$C_\rho = \frac{f_\rho^2}{m_\rho^2}\left[\frac{f_\pi^2}{m_\pi^2}\right]^{-1}. \tag{A11}$$

The expressions for the correlation functions are the following:

$$g_L(q) = -\left\{\boldsymbol{q}^2 + \frac{1}{3}q_c^2\right\}\tilde{F}_\pi^2(q)\tilde{G}_\pi^0(q) - \frac{2}{3}q_c^2 C_\rho\tilde{F}_\rho^2(q)\tilde{G}_\rho^0(q), \tag{A12}$$

$$g_T(q) = -\frac{1}{3}q_c^2\tilde{F}_\pi^2(q)\tilde{G}_\pi^0(q) - \left\{\boldsymbol{q}^2 + \frac{2}{3}q_c^2\right\}C_\rho\tilde{F}_\rho^2(q)\tilde{G}_\rho^0(q), \tag{A13}$$

$$g_L^\Lambda(q) = -\left\{\boldsymbol{q}^2 + \frac{1}{3}q_c^2\right\}\tilde{F}_\pi^2(q)\tilde{G}_\pi^0(q), \tag{A14}$$

$$g_T^\Lambda(q) = -\frac{1}{3}q_c^2\tilde{F}_\pi^2(q)\tilde{G}_\pi^0(q). \tag{A15}$$

Using the set of parameters

$$q_c = 780 \text{ MeV}, \quad \Lambda_\pi = 1.2 \text{ GeV}, \quad \Lambda_\rho = 2.5 \text{ GeV},$$

$$f_\pi^2/4\pi = 0.08, \quad C_\rho = 2, \tag{A16}$$

at zero energy and momentum we have

$$g_L(0) = g_T(0) = 0.615, \quad g_L^\Lambda(0) = g_T^\Lambda(0) = 0.155. \tag{A17}$$

However, we wish to keep the zero energy and momentum limit of $g_{L,T}$ and $g_{L,T}^\Lambda$ as free parameters; thus we replace the previous functions by

$$g_{L,T}(q) \to g'\frac{g_{L,T}(q)}{g_{L,T}(0)}, \quad g_{L,T}^\Lambda(q) \to g'_\Lambda\frac{g_{L,T}^\Lambda(q)}{g_{L,T}^\Lambda(0)}. \tag{A18}$$

[1] B. F. Gibson and E. V. Hungerford, Phys. Rep. **257**, 349 (1995).

[2] H. Outa *et al.*, Nucl. Phys. **A639**, 251c (1998).

[3] U. Straub, Z. Y. Zhang, K. Bräuer, A. Faessler, S. B. Khadkikar, and G. Lübeck, Nucl. Phys. **A508**, 385c (1990).

[4] U. Straub, J. Nieves, A. Faessler, and E. Oset, Nucl. Phys. **A556**, 531 (1993).

[5] J. Haidenbuaer, K. Holinde, K. Kilian, and T. Sefzick, Phys. Rev. C **52**, 3496 (1995).

[6] T. Kishimoto, Nucl. Phys. **A629**, 369c (1998).

[7] E. Oset and J. Nieves, Phys. Rev. C **47**, 1478 (1993).

[8] E. Oset and A. Ramos, Prog. Part. Nucl. Phys. **41**, 191 (1998).

[9] A. Parreño, A. Ramos, C. Bennhold, and K. Maltman, Phys. Lett. B **435**, 1 (1998).

[10] J. Cohen, Prog. Part. Nucl. Phys. **25**, 1 (1990).

[11] A. Parreño, A. Ramos, and C. Bennhold, Phys. Rev. C **56**, 339 (1997).

[12] T. Inoue, M. Oka, T. Motoba, and K. Itonaga, Nucl. Phys. **A633**, 312 (1998).

[13] J. F. Dubach, G. B. Feldman, B. R. Holstein, and L. de la Torre, Ann. Phys. (N.Y.) **249**, 146 (1996).

[14] K. Itonaga, T. Ueda, and T. Motoba, Nucl. Phys. **A585**, 331c (1995).

[15] W. M. Alberico, A. De Pace, M. Ericson, and A. Molinari, Phys. Lett. B **256**, 134 (1991).

[16] A. Ramos, E. Oset, and L. L. Salcedo, Phys. Rev. C **50**, 2314 (1995).

[17] A. Ramos, M. J. Vicente-Vacas, and E. Oset, Phys. Rev. C **55**, 735 (1997).

[18] E. Oset and L. L. Salcedo, Nucl. Phys. **A443**, 704 (1985).

[19] E. Oset, P. Fernández de Córdoba, J. Nieves, A. Ramos, and L. L. Salcedo, Prog. Theor. Phys. Suppl. **117**, 461 (1994).

[20] A. L. Fetter and J. D. Walecka, *Quantum Theory of Many Particle Systems* (McGraw-Hill, New York, 1971).

[21] E. Oset, P. Fernández de Córdoba, L. L. Salcedo, and R. Brockmann, Phys. Rep. **188**, 79 (1990).

[22] R. Seki and K. Masutani, Phys. Rev. C **27**, 2799 (1983).

[23] A. Parreño, A. Ramos, and C. Bennhold, Phys. Rev. C **52**, R1768 (1995); **54**, 1500(E) (1996).

[24] P. H. Pile *et al.*, Phys. Rev. Lett. **66**, 2585 (1991).

[25] T. Hasegawa *et al.*, Phys. Rev. C **53**, 1210 (1996).

[26] R. H. Dalitz and G. Rajasekaran, Phys. Lett. **1**, 58 (1962); M. M. Block and R. H. Dalitz, Phys. Rev. Lett. **11**, 96 (1963).

[27] E. Oset, H. Toki, and W. Weise, Phys. Rep. **83**, 281 (1982).

[28] J. J. Szymanski *et al.*, Phys. Rev. C **43**, 849 (1991).

[29] H. Noumi *et al.*, Phys. Rev. C **52**, 2936 (1995).

[30] C. B. Dover, A. Gal, and D. J. Millener, Phys. Rev. C **38**, 2700 (1988).

[31] J. Vidaña, A. Polls, A. Ramos, and M. Hjorth-Jensen, Nucl. Phys. **A644**, 201 (1998).

[32] H. C. Bhang *et al.*, Phys. Rev. Lett. **81**, 4321 (1998).

[33] Y. Sato *et al.*, Nucl. Phys. **A639**, 279c (1998).

[34] P. Kulessa *et al.*, Phys. Lett. B **427**, 403 (1998).

[35] T. A. Armstrong *et al.*, Phys. Rev. C **47**, 1957 (1993).

[36] H. Ohm *et al.*, Nucl. Phys. **A629**, 416c (1998).

[37] H. Outa (private communication).

[38] V. J. Zeps, Nucl. Phys. **A639**, 261c (1998).

[39] M. Agnello *et al.*, Nucl. Phys. **A639**, 537c (1998).